Developmental Biology 462 (2020) 50–59

Contents lists available at ScienceDirect

Developmental Biology

journal homepage: www.elsevier.com/locate/developmentalbiology

Original research article

Space colonization by branching trachea explains the morphospace of a simple respiratory organ

A. Ruiz-Sobrino [a,1], C.A. Martín-Blanco [a,1], T. Navarro [a,1], I. Almudí [a], G. Masiero [a], M. Jiménez-Caballero [a], D.B. Buchwalter [c], D.H. Funk [d], J.L. Gattolliat [e,f], M.C. Lemos [b], F. Jiménez [b,2], F. Casares [a,*,2]

[a] CABD, GEM-DMC2 Unit (CSIC-Pablo de Olavide University-Junta de Andalucía), 41013, Seville, Spain
[b] Department of Condensed Matter Physics, University of Sevilla, 41012, Sevilla, Spain
[c] North Carolina State University, Department of Biological Sciences, Raleigh, NC, 27695, USA
[d] Stroud Water Research Center, Avondale, PA, 19311, USA
[e] Musée Cantonal de Zoologie, CH-1014, Lausanne, Switzerland
[f] University of Lausanne (UNIL), Department of Ecology and Evolution, CH-1015, Lausanne, Switzerland

ARTICLE INFO

Keywords:
Branching morphogenesis
Mayfly gill
Cloeon
Space colonization algorithm
Computational models
Branchless
Fibroblast growth factor

ABSTRACT

Branching morphogenesis helps increase the efficiency of gas and liquid transport in many animal organs. Studies in several model organisms have highlighted the molecular and cellular complexity behind branching morphogenesis. To understand this complexity, computational models have been developed with the goal of identifying the "major rules" that globally explain the branching patterns. These models also guide further experimental exploration of the biological processes that execute and maintain these rules. In this paper we introduce the tracheal gills of mayfly (Ephemeroptera) larvae as a model system to study the generation of branched respiratory patterns. First, we describe the gills of the mayfly *Cloeon dipterum*, and quantitatively characterize the geometry of its branching trachea. We next extend this characterization to those of related species to generate the morphospace of branching patterns. Then, we show how an algorithm based on the "space colonization" concept (SCA) can generate this branching morphospace via growth towards a hypothetical attractor molecule (M). SCA differs from other branch-generating algorithms in that the geometry generated depends to a great extent on its perception of the "external" space available for branching, uses few rules and, importantly, can be easily translated into a realistic "biological patterning algorithm". We identified a gene in the *C. dipterum* genome (*Cd-bnl*) that is orthologous to the fibroblast growth factor *branchless (bnl),* which stimulates growth and branching of embryonic trachea in *Drosophila*. In *C. dipterum*, this gene is expressed in the gill margins and areas of finer tracheolar branching from thicker trachea. Thus, *Cd-bnl* may perform the function of M in our model. Finally, we discuss this general mechanism in the context of other branching pattern-generating algorithms.

1. Introduction

Branching patterns are pervasive in nature and essential to the efficient distribution of liquids and gasses in biological systems. Within animals, branching tubular systems are found in organs as diverse as lungs, kidneys, blood vessels, mammary glands and insect trachea, where they increase the functional surface area for gas or liquid exchange. In general, the branching patterns found in these organs show complex, self-similar tri-dimensional geometries (Varner and Nelson, 2017). When studied at the molecular and cellular detail, the mechanisms generating the respiratory trees in mouse or in *Drosophila* seem exceedingly complex (Metzger et al., 2008). For example, in the *Drosophila* embryo Ghabrial and co-workers found in a genetic screen over 200 patterning/morphogenetic genes, beyond house-keeping genes, that were necessary for shaping and developing the arborization of the tracheal system (Ghabrial et al., 2011). To understand this complexity, models aimed at achieving a

* Corresponding author.
E-mail addresses: jimenez@us.es (F. Jiménez), fcasfer@upo.es (F. Casares).
[1] These authors contributed equally.
[2] Senior authors.

https://doi.org/10.1016/j.ydbio.2020.02.005
Received 31 July 2019; Received in revised form 29 January 2020; Accepted 4 February 2020
Available online 25 February 2020

systems-level understanding have been developed. The goal of these models is to identify the minimal set of processes that are capable of generating and maintaining the branching pattern. This global understanding, rather than an understanding of the individual parts, may be then used to focus further research on the mechanisms of those essential processes, aiding in posing the relevant experimental questions. In addition, the branching morphogenesis of an organ may vary depending on environmental conditions, or between homologous organs in related species (e.g. mouse and human). Therefore, these models should also help explain in the most parsimonious manner how the phenotypic plasticity of a branching pattern and its evolutionary variation (i.e. the pattern's *morphospace*) may arise.

Models of animal branching morphogenesis fall into three major categories (reviewed in (Varner and Nelson, 2017; Iber and Menshykau, 2013)). The realization of the self-similar or fractal nature of these patterns (Mandelbrot, 1983; Glenny, 2011) led to the development of geometric models using recursive algorithms to quantitatively reproduce the general geometry of the lung's arborization and its interspecific variation (Nelson and Manchester, 1988; Nelson et al., 1990; Kitaoka and Suki, 1997). However, for these types of models it is often difficult to link the recursive rules of the patterning-generating algorithm to the biological causes. To address this limitation, a second class of models, of reaction-diffusion type, has been developed that link local geometry and gene regulatory networks. Therefore, in these models, molecular details are included that allow for the investigation of the initiation of the branching process, such as bronchial budding and elongation (Kondo and Miura, 2010; Menshykau et al., 2014) and the branching pattern of the kidney ducts (Menshykau et al., 2019). A third class is that of models that investigate the role of mechanical forces as agents in the branching process and, in general, have a focus on the biomechanical properties of

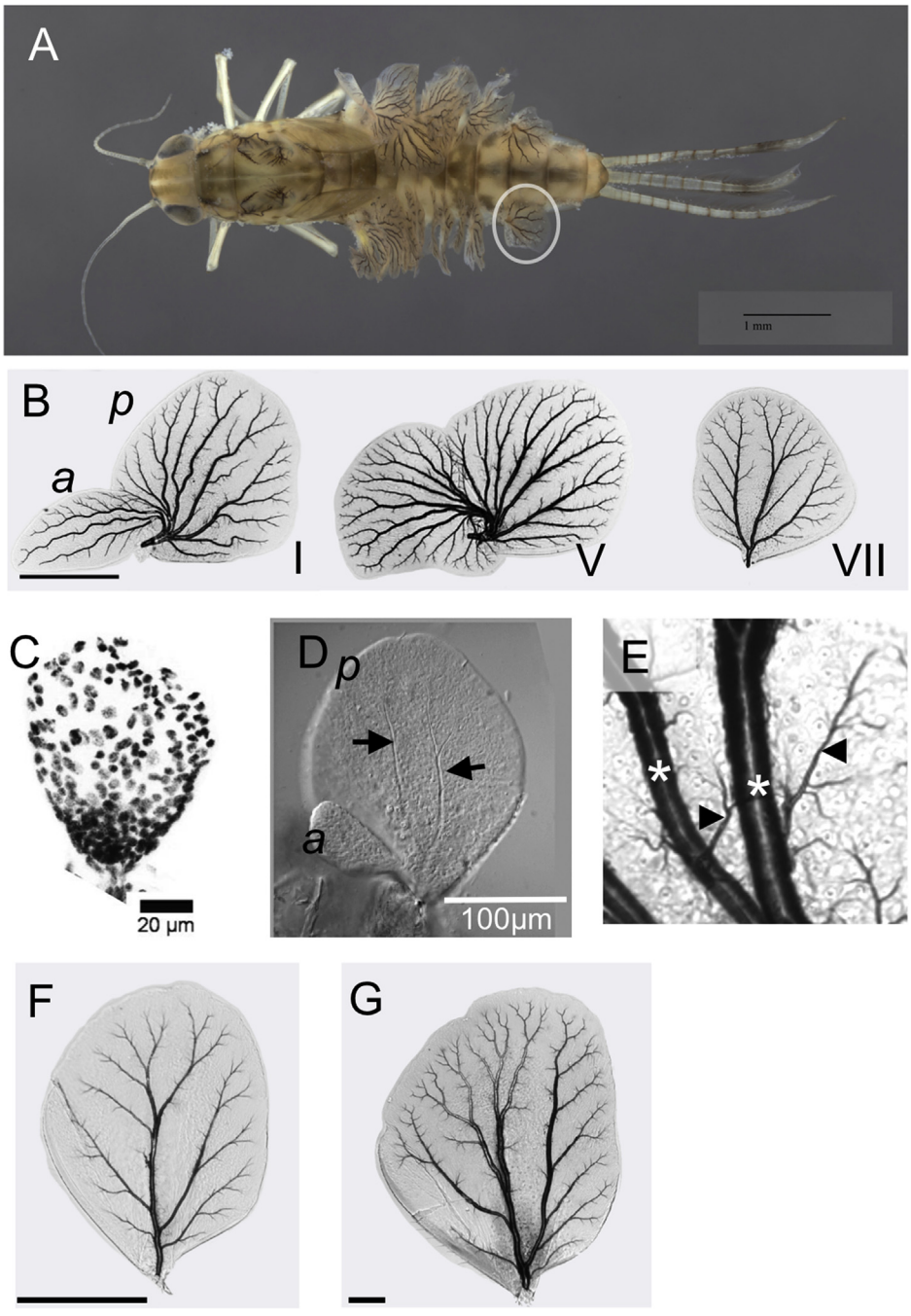

Fig. 1. The tracheal gills of the mayfly *Cloeon dipterum* and the development of their arborization. (A) The aquatic nymph bears gills on its first seven abdominal segments. The white ellipse marks one of them. Scale bar is 1 mm. (B) Microscopic images of abdominal gills 1, 5 and 7. Except for the pair on abdominal segment 7, gills are bilamellate. The scale bar in (B) is 500 µm. (C) DAPI stained gill IV of a 5 day old nymph. No signs of trachea are visible yet. (D) Bright field micrograph of a 13 day old nymph gill III where the trachea (arrows) have invaded the epithelial parenchyma of the posterior lamella (p) through its base. The anterior lamella (a) is already visible stemming from the base of the posterior one. (E) In later stages, small tracheoles (arrowheads) branch out from thicker, older trachea (asterisks). (F–G) Gills VII (from different individuals) at 34 (F) and 38 (G) days post-hatching. Scale bars are 100 µm. The branching pattern scales with growth (note that the length/width of the gill approximately doubles from F to G and includes further elaborations, mostly distally).

the tube structures as emerging from cell- and tissue-level properties (see, for example (Kim et al., 2013),). It is clear that elements of all three modeling approaches are critical to developing a robust understanding of branching morphogenesis and should be combined when possible. For example, a recent geometry-based model, that also incorporates molecular information on relevant intercellular signaling processes, has been used to explain the global morphology of the branched ducts of the mammary gland (Hannezo et al., 2017).

Still it is not clear yet whether the mechanisms identified by these models are universal –e.g. whether they can explain the branching patterns of both ductal systems, which are specialized in liquid transport, and those of the respiratory arborizations of lungs or insect trachea that transport gases– or to what extent they are able to generate the developmental plasticity and the evolutionary diversity of these patterns. In this paper, we capitalize on the branching patterns of trachea in the mayfly gill to investigate the global mechanism that drive their generation and morphological evolution.

2. Results

2.1. The branching pattern and morphology of the tracheal gills of Cloeon and other mayflies

The aquatic nymphs of the Baetid mayfly *Cloeon dipterum* bear respiratory gills on abdominal segments I to VII. These gills are movable, flat epithelial bilayers (Fig. 1) traversed by ramifying trachea (Craig, 1990; Riek, 1973). In their structure and function, they are similar to a small bi-dimensional lung, with gas being exchanged between the thin distal trachea (secondary trachea) and the surrounding water through the epithelium as gas is exchanged between the alveoli and the blood through the capillary endothelium. Gills on segments I to VI are bi-lamellate, while those on segment VII are uni-lamellate (and the only non-movable gill pair) (Fig. 1B). *Cloeon* gills are oval shaped and generally considered to be of the ancestral type (Riek, 1973; Kukalova-Peck, 1985) (Fig. 1B). Gills start developing on the second nymphal stage and soon thereafter trachea invade the pad and start branching (Fig. 1C,D). The onset of gill development coincides with some other developmental processes, such as the growth of the medial cercus and the wing pads. Globally, trachea diameter thins as the tubes get close to the periphery of the gill (distal portion). Also, and as development proceeds, new thin tracheae branch out from thicker, more internal (proximal) segments (Fig. 1E). Therefore, tube thickness can be considered a correlate of branching time –with thinner tubes having branched more recently. Tracheal branching is asymmetric and trachea do not anastomose. As the gills grow, their pattern scales (Fig. 1F,G). Although left and right gills from the same abdominal segment are similar to each other, they are not identical, indicating that the specific branching pattern is not totally deterministic (not shown). Globally, mayflies show a large variation in overall gill number, morphology and branching pattern (Riek, 1973): the shape of the gills (fibrillose, bifurcate, spine-like, operculate...) is recognized as being of phylogenetic importance. Besides respiration, gills can have additional functions such as osmoregulation, substrate attachment forming a sucking disc (in *Rhithrogena*) or mechanical protection (opercula in Caenidae, Leptohyphidae, Coryphoridae and others). Gills can be secondarily very reduced or even completely absent (*Murphyella*). Fig. S1 shows a sample of gills from several related mayfly species that show a variety of branching patterns. One expectation from a biologically relevant patterning system is that it should be capable of generating this natural morphospace of branching patterns by small modifications in its parameters.

2.2. The space colonization algorithm (SCA) generates branching patterns similar to those of biological gills

Since we still lack even a basic molecular understanding of gill development in mayflies, the approximation used in this work to understand the generation of this branching patterns has been macroscopic: trying to identify a simple algorithm that generates patterns similar to those of natural gills and, at the same time, which could be translated into the smallest possible set of biological mechanisms. The superficial resemblance of this pattern to a branching tree or root system set us to search for tree-generating algorithms. Most algorithms generating branched patterns are based on "recursive branching": a series of rules that specify branching frequency, angles and relative branch length. These are all "internal" rules. However, Runions and colleagues, aiming at computer-drawing realistic tree- and shrub-like structures, used an alternative concept: "space colonization" (Runions et al., 2005, 2007). The fundamental difference with other branching-generating algorithms is that the geometry generated depends to a great extent on its perception of the "external" space available for growth. In brief, the space colonization algorithm works as follows (Fig. 2): The space to be colonized by the branching structure is filled with attractive points (M); A branch will grow at a speed (*CREC*) towards M if it is within a certain distance from M (*MAX*: radius of influence) (or towards the mean position of several Ms when the branch is within the reach of these Ms). The points are then removed as the branch reaches closer to these points (within a "killing" radius, *KILL*). The starting point of the branching structure is a single node in the space filled with M attracting points ("root"), and the structure finishes when all these attracting points have been eliminated. Therefore, "available space" is perceived as remaining attracting points. We have implemented a 2D SCA algorithm in which the shape of the space to be colonized can be set to an ellipse, as a first approximation to the gill shape, or to any other (polygonal) shape. In addition, branching proceeds within a growing space. Although in its original form M points are placed at specific locations to determine final tree shape, in our implementation Ms are distributed randomly at a user-controlled density and, in addition, the position of each M can be affected by a stochastic motion (random walk, at speed *vel,* making it a *dynamic* space colonization algorithm, or *dSCA*). (Fig. 2A; see also Methods for the algorithm's pseudo-code and Supplementary Material for detailed descriptions). Fig. 2B-B'' shows three time points in the development of a "synthetic gill" generated by this SCA implementation. Branching proceeds outwards, asymmetrically, and without crossings, recapitulating the pattern of a "natural" gill. In what follows, we develop a series of metrics to compare, first, between natural and synthetic gills, to then study how some major parameters affect their geometry.

2.3. Geometric characterization of gill branching patterns

In order to characterize the branching geometry of gills, we proceeded in three steps. First, we developed a pipeline for image segmentation (see Materials and Methods and Supplementary Material) that resulted in skeletonized images where every branch has a pixel width and branching nodes and branch tips are located in the image (Fig. S2A). Second, we developed a battery of metrics to quantify the differences we are able to detect visually between branching patterns across species (Materials and Methods). Each of these metrics defines some aspect of the pattern and was developed when a previous metric was unable to discriminate between two patterns. For example, we started by defining "branch density" (branching pixels relative to total pixels (i.e. gill surface)) as a metric able to differentiate some patterns. However, it is easy to imagine two different patterns with identical branch density (Fig. S2B). Then, a new one metric, "Branch tips" (tips to surface ratio), is now able to differentiate them (Fig. S2B). Following this logic, we developed a series of 8 metrics that characterize the branching geometry (see Materials and Methods for full description), including its fractal dimension. However, in a given dataset it may be that some of these metrics are partly redundant (i.e. there is correlation between them). In this case, the comparison of two or more gill sets can be done using Principal Component Analysis (PCA), so that the variability between sets leads to the selection of a specific linear combination of metrics that is used to compare the patterns.

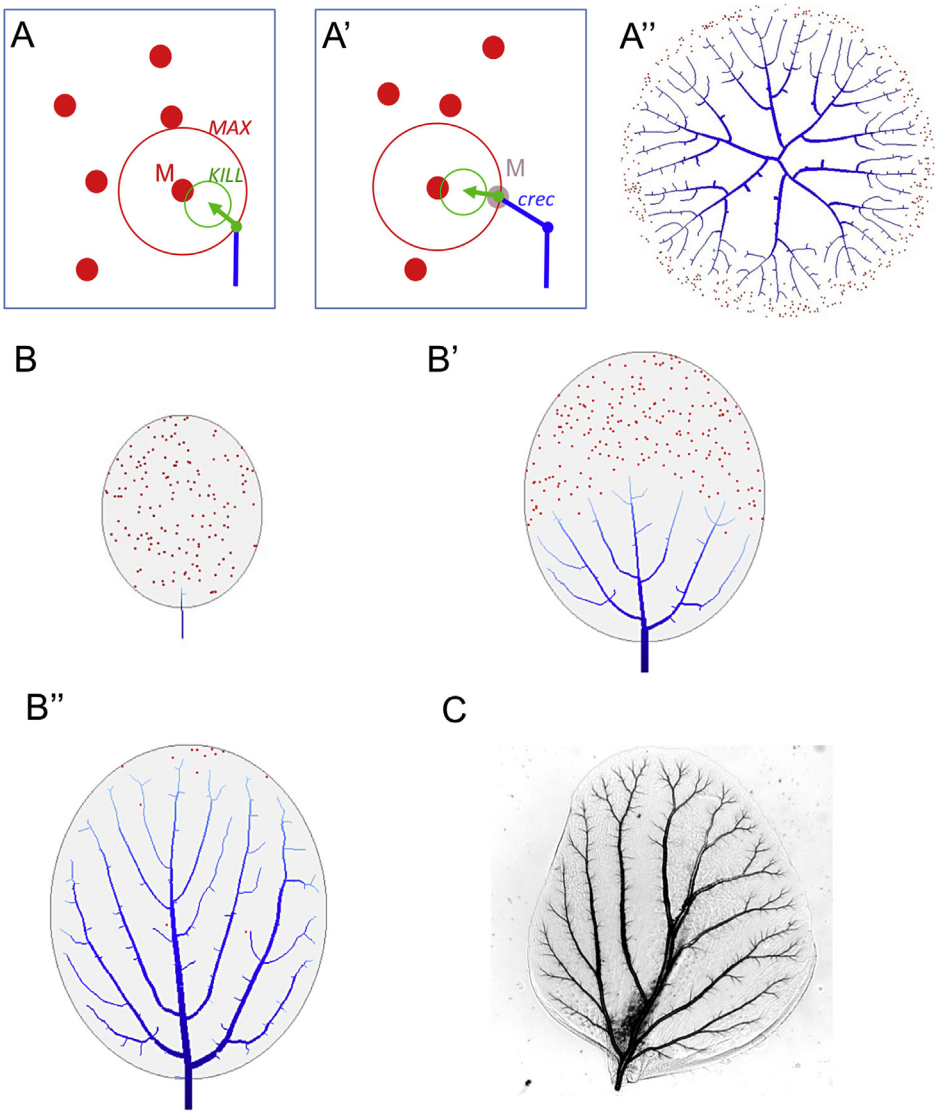

Fig. 2. An algorithm based on Space Colonization generates realistic gill branching patterns. The space colonization algorithm (SCA; A-A''): (A) A segment (blue) that falls within the radius of influence of an attracting point "M" grows in this direction. When the segment is close enough to the point, the point is eliminated. The process continues (A') as long as there are more attracting points within reach. "MAX" is the radius of influence of M (i.e. the distance at which the segment can detect M), "KILL" is the radius of "killing" (or erasure) of M and "crec" is the increase in length of the branch per iteration. (A'') The SCA algorithm, with a seed located in the center of a space filled with M points (red), generates a branching pattern (blue). (B–B'') Three time-points along the development of a SCA-generated "synthetic" gill. M points in red. The younger the branches, the lighter the blue color. (C) A "natural" *Cloeon* VII gill is shown for comparison.

The two principal components explain a large fraction of the variability (Fig. S2C and Supplementary Materials) and were renamed as "richness" (x) and "irregularity" (y) (Fig. 3). "Richness" reflects the density of different elements (nodes, tips and density mainly) while "irregularity" reflects the degree of heterogeneous branch lengths and unequal distribution of nodes of the pattern. Fig. 3 represents the distribution of natural gills according to these two principal components. In this morphospace the richer sampling is of *Cloeon dipterum, Baetis (Rhodobaetis) tenerifensis* and *Siphlonurus quebecensis,* for which we analyzed all abdominal gills (A1 to A7) from one individual per species, including the small lamellae (A1-A6 in *Cloeon* and A1 and A2 in *Siphlonurus*) (Fig. S3), but it also includes gills from other species (see phylogenetic tree in Fig. S1). The metrics can vary one order of magnitude between different patterns. For example, the density of tips per gill ("branch.tips") is one of the metrics that contributes the most to the "richness" component and ranges from 5×10^{-3} to 2×10^{-4} between *Alainites* and *Siphlonurus,* this latter the species with the "richest" patterns in our sample. Within the second component, "irregularity", "average number of ancestors" measures how the nodes distribute along a branch and ranges from 0,18 in *Alainites* to 1,86 in *Neocleon.* Globally, this quantitative analysis allows the discrimination of different branching patterns and describes the gill morphospace of our sample of species.

2.4. Exploration of SCA-generated branching patterns

In order to explore the range of branching patterns generated by the SCA algorithm, we simulated synthetic gills varying one of these parameters at a time. As availability of M is key, as it defines "unoccupied space", we first studied the effects of varying M concentrations. As expected, the total branch length saturates as [M] increases. More interesting is the fact that, at intermediate concentration the pattern varies quickly, from sparse and undulated (that we have not observed in nature, as in all species examined trachea grow straight) to patterns resembling natural gills (Fig. 4A). Therefore, within a range of M, relatively small variations in M can result in qualitatively different patterns. Another parameter is gill morphology. However, when synthetic gills differing only in their ellipticity (i.e. with all dSCA parameters remaining equal) were generated, the resulting branching patterns are qualitatively similar (Fig. 4B). Finally, we explored varying the two radii, *MAX* (detection of M) and *KILL* (the radius of killing of M). While MAX above 40 generate similar realistic patterns without much qualitative change (Fig. 4C), decreasing KILL increases the richness of the arborization (Fig. 4D).

In order to statistically assess the discrimination power of our PCA analysis, we took the 3 species with the largest sample size (*Cloeon, Baetis* and *Siphlonurus*) and compared them through different methods (see

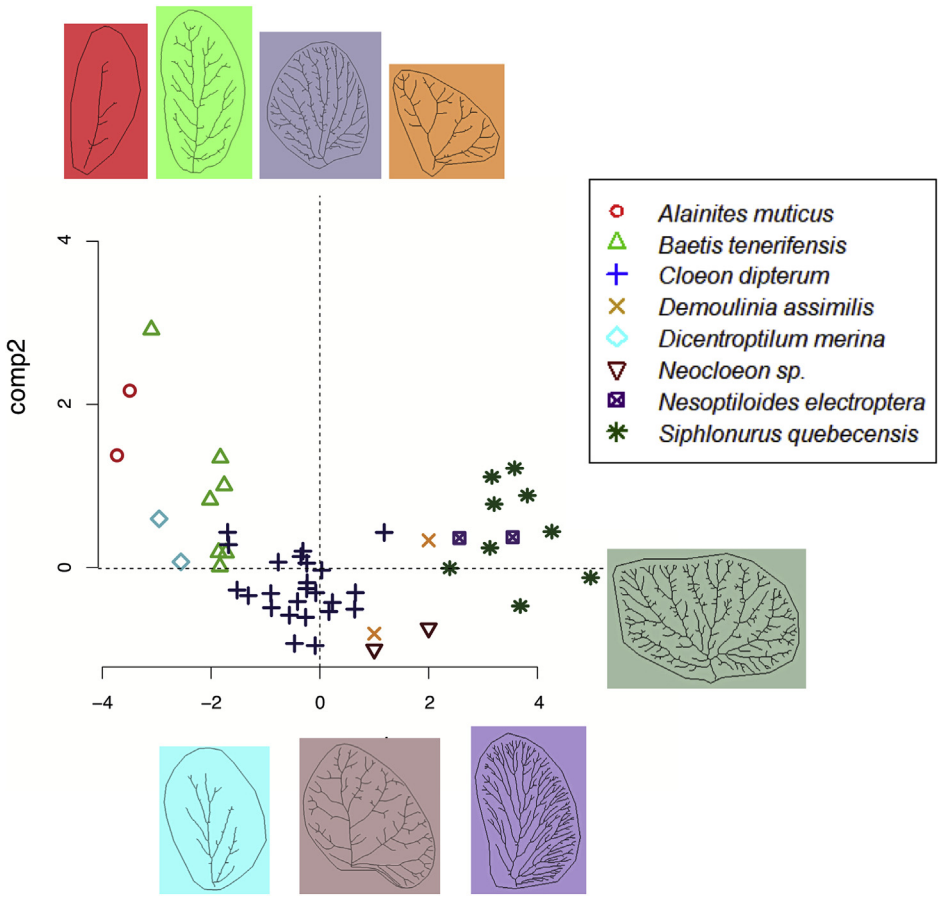

Fig. 3. Natural morphospace of the gill branching patterns. Distribution of the species according to the two principal component analysis. A sample skeletonized image for each species, color-coded, is included. Gills of different species fall in different regions of this morphospace.

Materials and Methods for details). First, we performed an unrestricted multinomial regression model to test whether the values of the two first PCA components of each gill pattern (alone or in combination) were able to predict the species this pattern belonged to. The model using the combination of Comp.1 and Comp.2 was a perfect classifier of species, with 100% of success in predictions (see Table S1). When each PCA component was tested alone, even the Comp.1 is enough for a perfect discrimination among these groups, while Comp.2 predicted the species correctly with a 72.5% of success. Therefore both components are sensitive enough for species-specific gill pattern discrimination. Finally, just working with Comp.1, an ANOVA analysis was performed to confirm Comp.1 means are significantly different between the 3 groups (p-value~0) and significant too in pairwise comparisons (Adjusted p-value~0). Therefore, the morphospace described by our PCA analysis is capable of discriminating the different species-specific patterns in a statistically significant manner.

2.5. The range of SCA-generated patterns covers the natural morphospace

To have a clearer idea of the impact each parameter had on the pattern, and to compare synthetic and natural gills, we quantified and represented their metrics within the two-components morphospace (Fig. 5). We found that variations in the SCA parameters generated patterns that cover the whole range of branching patterns in the species we have surveyed, from simple and irregular (such as some found in *Baetis tenerifensis*) to more complex and ramified (like those of *Siphlonurus quebecencis*). An especially sensitive parameter is KILL, the distance at which a growing branch erases the attracting M: reducing the KILL radius results simultaneously in richer and more irregular patterns. Therefore, a space colonization algorithm reproduces quantitatively the geometry of the whole morphospace of natural gills we have analyzed. The full set of images (natural gills and SCA generated patterns) and extracted datasets are provided as Supplementary Material. Software (segmentation macros, raw metrics generating algorithm and spatial colonization algorithm) is available through GitHub (see Supplementary Materials).

2.6. Cloeon FGF is expressed in uncolonized areas of the gill

The FGF ligand *branchless (bnl)* is known to stimulate the growth and branching of embryonic trachea and the thoracic air sac primordium in *Drosophila* (Metzger and Krasnow, 1999; Sato and Kornberg, 2002). Therefore, *bnl* could be, in principle, a good candidate for M. However, in both instances *bnl* is produced at specific sites to direct tracheogenesis, while our model does not require M transcription to be actively patterned. Instead, the pattern arises from the repressing action of growing trachea. Therefore, our model predicts M to be transcribed along the margin of the gill (where most of the finer trachea are growing into) and in the inter-trachea regions with lowest branching density. To test this prediction, we identified the *bnl* orthologue in *Cloeon dipterum's* genome (Almudi et al., 2019a, 2019b) (Fig. s4 and Table S2) with which we generated an anti-sense probe. *In situ* hybridization revealed that indeed *Cd-bnl* is expressed most strongly along the margin, where the tips of trachea are growing, and around the fine tracheoles branching from thicker tubes, in the gill internal regions (Fig. 6). Indeed, this pattern is compatible with the pattern expected for M in the SCA algorithm (see Fig. 2B''), which should be present in regions not yet colonized (or in the process of being colonized) by trachea.

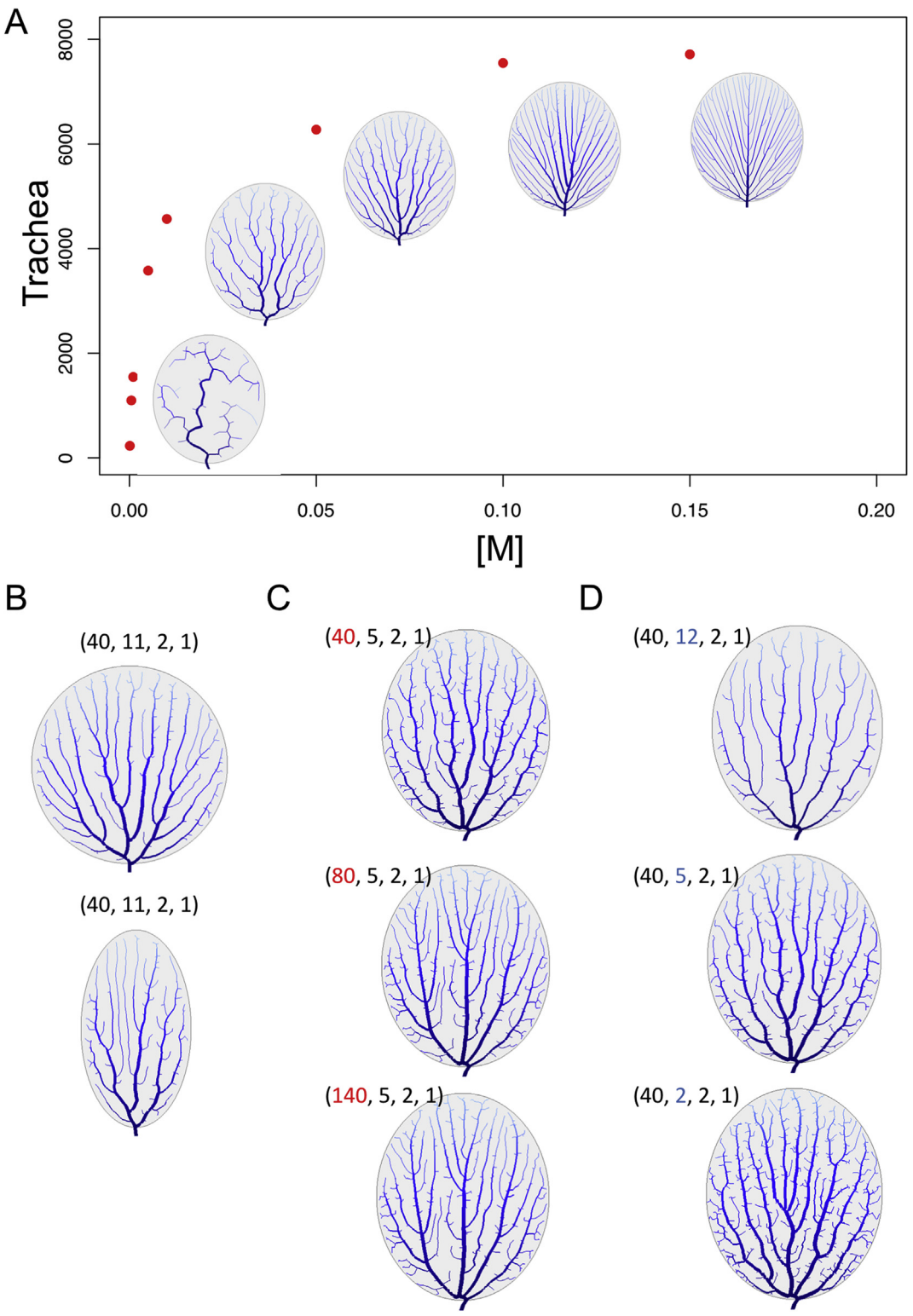

Fig. 4. Effects of M and global shape on gill branching pattern. (A) Effect of increasing M concentration (M/pixels) on total trachea length. Parameters (40,11,2,1) (MAX, KILL, CREC, vel), constant shape (semiaxis (a,b)= (200,230). Red dots, simulations. Some graphic outputs ("synthetic" gills) are shown. (B) Effects of varying ellipticity (short semiaxis/long semiaxis of B1 = 128/230 and of B2 = 228/230) using (MAX, KILL, CREC, vel)= (40, 11, 2, 1), as in (A). (C) Variation of MAX. (D) Variation of KILL.

3. Discussion

In what follows we will try to translate our implementation of the SCA algorithm into plausible biological processes. Although our model is not molecularly specific, we will draw hypotheses on potential molecular mechanisms from the model and from prior research. Finally, we will compare the space colonization model with previous models explaining tubular branching patterns to highlight the most important differences.

The space colonization algorithm is based on very simple rules: attracting molecules, M, direct the growth/branching of trachea which,

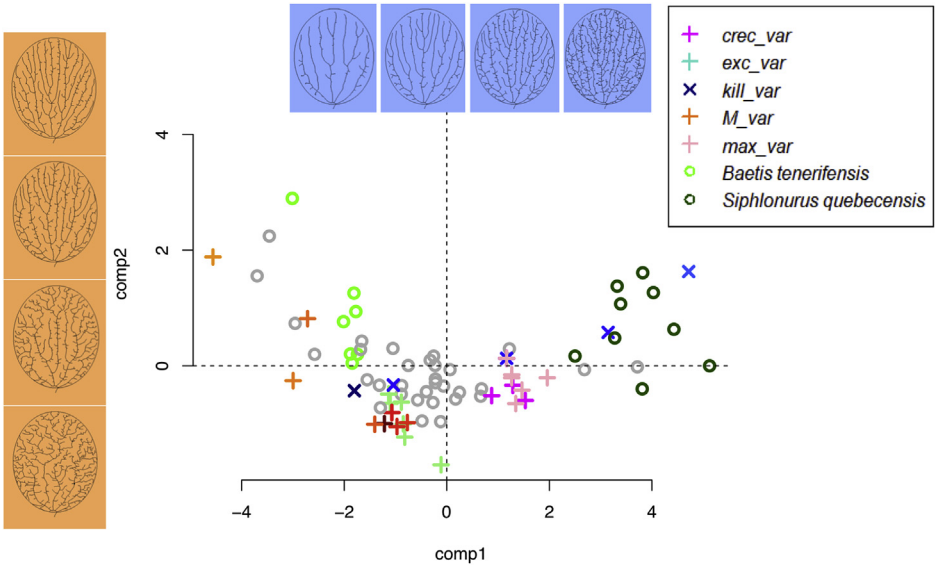

Fig. 5. Variations in parameters and their effects on branching geometry. Plot of the PCA analysis including natural gill patterns (grey circles, data in Fig. 3) and simulated patterns varying the main SCA parameters. Skeletonized images shown are variations in *KILL* (top row, from left to right: 40,20,2,1; 40,12,2,1; 40,5,2,1; 40,2,2,1; blue symbols) and variations in *CREC* (left, column, top to bottom: 40,5,1,1; 40,5,2,1; 40,5,4,1; 40,5,8,1; orange symbols). Other simulations include variations of shape (ellipticity, *exc,* green), *MAX* (30,5,2,1; 40,5,2,1; 80,5,2,1; 100,5,2,1; 200,5,2,1; 250,5,2,1; pink symbols) and *M* (as in Fig. 4). The circle symbols are *Baetis* (light green) and *Siphlonurus* (dark green) gills.

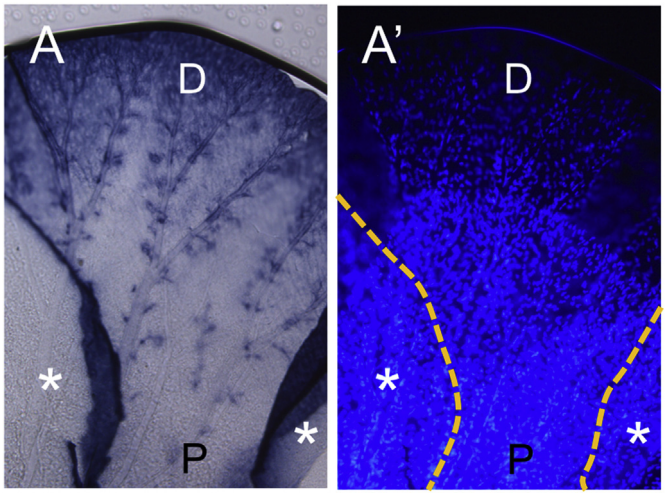

Fig. 6. Expression pattern of *Cloeon bnl* in gills. (A) White field image of a gill hybridized with an anti-sense bnl/FGF probe. The signal is stronger along the margin, where the distal tips of the growing trachea are located. In addition, signal is detected at, or around, the finer tracheoles in the inner region of the gill. (A′) DAPI staining of the same gill to visualize cell nuclei. (*) indicates lateral gill regions still covered by cuticle. The cuticle precludes staining. "P" and "D" mark "proximal" and "distal", respectively. (See Fig. S4 and Supplementary Materials and Methods for further details on *Cloeon dipterum bnl* sequence identification).

when reaching closer, eliminate these attracting Ms. This algorithm results in a directional growth of the pattern and yet it does not require external sources of positional information, such as signaling centers or gradients: M would be distributed uniformly and the arborization will grow from its root -the entry point of the trachea into the gill. "[M]" denotes an *effective* concentration, not the actual concentration of the molecular attractant. For example, higher M might reflect an increase in the *affinity* for M in tracheal cells. We obtain realistic patterns for *MAX* ≥ 40 px -with minimal effects on the pattern with values above 4o px. Since our *Cloeon* images are calibrated, with 1 px = 1,69 μm, the model predicts an M's range of action (*MAX*) ≥ 70 μm for the molecule that incarnated M.

When trachea approaching M reach a *KILL* distance, M is erased. Molecularly this would be equivalent to a repression of M production or the reception/degradation of M by the arriving tube, acting as a sink. In *Drosophila* embryos, tracheal cells have been shown to explore their surroundings by means of thin cellular extensions called filopodia (Ribeiro et al., 2002). Similar extensions could be used by mayfly trachea to survey the gill and detect M to either produce a local inhibitor of M expression or to remove it from the media via receptor binding -or both. The length of *Drosophila* tracheal filopodia, as observed *in vivo,* can reach up to 20 μm ((Ribeiro et al., 2002), see also (Okenve-Ramos and Llimargas, 2014)). Our model yields realistic branching patterns for values of *KILL* between 2-12 px (with larger values giving rise to fewer lateral ramification; Figs. 4 and 5). Using the 1 px = 1,69 μm equivalence, *KILL* values of 2–12 px are then equivalent to 3–20 μm, which are well within the range of *Drosophila* filopodia lengths observed *in vivo*.

The role played by FGF ligands in the growth and branching of *Drosophila* tracheae and bronchial buds in lungs makes this family of ligands good candidates to incarnate M. As was mentioned above, while in *Drosophila bnl* is produced at localized sites, our model does not require active patterning of its expression. Indeed, the pattern of *bnl* transcription we detect in developing gills is the one expected to result from widespread transcription and local repression by growing trachea. Interestingly, even though initial work suggested that *localized* FGF10 production in the lung mesenchyme was necessary for normal branching (Metzger and Krasnow, 1999), later research showed this localization not to be required, as uniform FGF10 also supported normal bronchial patterning (Volckaert et al., 2013; Nogawa and Ito, 1995). Therefore, active patterning of *bnl/FGF* transcription might not be an absolute need for the generation of a branching pattern.

Recently Hannezo, Scheele and co-workers put forward a powerful model for branching morphogenesis, based on Branching and Annihilating Random Walks (BARWs), to explain the branching morphogenesis of the ductal systems of the mammary gland and the kidney (Hannezo et al., 2017). In the Hannezo-Scheele model, branching geometry arises through stochastic branching at the tip of the tubes (as opposed to more proximal regions which cannot branch) plus random exploration of space through tip elongation. The density of branching is controlled by inhibition, with tips turning irreversibly inactive in the proximity of other branches. Molecularly, elongation and branching are stimulated by FGF10, and tip cell activity (responsible for duct elongation and branching) is inhibited by TGF-β ligands produced by ducts in the vicinity of a tip. Our model, based on space colonization, differs in several aspects: exploration of space is systematic, rather than stochastic, with tracheal cells scanning a mean distance around them. In this sense, elongation and branching is "directed" towards unoccupied space. In our

model there is no need to define a tip cell as opposed to a trunk/stalk cell type: All points along the trachea are equally competent in elongation and branching. This allows trachea to keep colonizing the new M-producing space that arises as the gill grows, which results in a constant scaling of a self-similar pattern. Then, and in contrast to the Hannezo-Scheele model, elongation and branching do not occur as a default state, but only if there is available M (i.e. "space"). In this sense, the SCA model does not require a "tip-inhibition rule", as elongation/-branching halts once space has been occupied. Therefore, the SCA model is able to generate tracheal branching patterns with a minimum of parameters and rules.

One important feature of our model is that it can easily generate the morphospace of natural branching patterns. Among the parameters that seem to influence the pattern the most are *CREC* and *KILL*. *CREC* reflects the speed of tracheal elongation (per iteration). *KILL* represents the range at which the tracheal cells are able to repress/consume M. Both parameters thus reflect rates of cellular activity that may be easily modulated biologically. For example, variations in *CREC* might reflect the speed of tracheal elongation *relative* to gill growth. And *KILL* might be modulated by the length of the exploring filopodia. In addition to the branching pattern, gills vary largely in their overall shape, from very elongated (e.g. *Baetis*), through rounder (e.g. *Cloeon*) to very asymmetric (e.g. *Siphlonurus*). Overall shape does not seem to affect the geometry of the branching pattern and we suggest that gill shape may be controlled independently of the branching mechanism, likely through the regulation of growth rates and of the polarity of cell division.

In summary, a model based on space colonization is capable of explaining the generation of a whole morphospace of mayfly respiratory gills with a minimum of rules and parameters. Our model predicts that the attracting M does not need to be spatially localized and that, above a certain threshold, the precise regulation of its concentration is not critical. Instead, cellular parameters, such as elongation rates and efficiency of repressing/capturing or degrading the attractant by the trachea are much more important. Although our model is not molecularly specific, the similarities between the tracheal system in the insect model *Drosophila* and other branching patterns in vertebrates (Metzger et al., 2008; Metzger and Krasnow, 1999; Sato and Kornberg, 2002; Spurlin and Nelson, 2017; Ochoa-Espinosa and Affolter, 2012; Davies, 2002) (Almudi et al., 2019a, 2019b; Ribeiro et al., 2002; Okenve-Ramos and Llimargas, 2014; Volckaert et al., 2013), make FGF a good candidate for M, a chemoattractant directing the elongation/branching of the trachea. The expression pattern of *Cloeon bnl* is compatible with this model. Exploring this mechanism in other branching structures may help in gaining a global understanding of their generation and of the changes necessary for the morphological variation of these branching structures.

4. Materials and methods

Cloeon dipterum culture. A continuous culture of *Cloeon dipterum* is maintained in the Casares laboratory (CABD) (as described in (Almudi et al., 2019a; Sweeney et al., 2018)). *Cloeon* nymphs were fixed 20 min at room temperature in 4% formaldehyde (in phosphate buffer saline, pH 7, 2 (PBS)). After rinsing 3X in PBS, dissected *Cloeon* gills were mounted in glycerol 80% (in PBS) and imaged under a Leica DM5000 B microscope equipped with a Leica DFC 490 digital camera. Images were acquired as 512 × 512 pixel images in "tiff" format.

Siphlonurus quebecensis was reared in the laboratory using techniques similar to those described in (Sweeney et al., 2018). Fresh exuviae from the final nymphal instar were recovered immediately following emergence of the subimago. At this molt, tracheae within the gill are shed and remain air-filled. Gills were removed individually and placed in a temporary slide mount in water, then photographed with a Canon T1i camera body mounted on a Nikon Labophot-2 microscope using a 4x objective and a 2.5x projection eyepiece.

Gills of additional taxa (Figs. 3 and S1) were removed from specimens housed in the collection of the Museum of Zoology, Lausanne. Gills were mounted on slides in Euparal medium and photographed using an Olympus BX51 stereoscopic microscope with an Olympus SC50digital camera.

Image segmentation. Digital images were processed with ImageJ2 (Rueden et al., 2017). Briefly, the images are oriented, so that the gill root (tracheal entry point) is placed at the bottom of the image; then, the image is segmented using the "Trainable Weka Segmentation" ImageJ plug-in (Arganda-Carreras et al., 2017). Then the resulting image is manually corrected and skeletonized. Next, the perimeter of the gill is extracted using the "Polygon" tool and combined with the skeletonized image (i.e. branching pattern). We have programed a series of Macros tools for ImageJ to facilitate the segmentation process (see Supplementary Methods for a more detailed description of these Macros). The number of gills analyzed were: *Cloeon dipterum:* 24 (from a single individual, comprising large and small lamellae); *Siphlonurus quebecensis:* 9 (from a single individual); *Baetis tenerifensis:* 7; *Alainites muticus:* 2; *Neocloeon* sp.: 2; *Demoulinia assimilis:* 2; *Dicentroptilum merina:* 2; *Nesoptiloides electroptera:* 2.

In situ hybridization on Cloeon gills. First, nymphs were fixed with Formaldehyde 4% in PBS (overnight, 4 °C) and then rinsed (3 × 10′ PBT (PBS, 0,3%TritonX-100)). To allow for reagents penetration, the cuticle of the gill is removed with forceps under a stereomicroscope (usually the cuticle on the posterior side), and then the gill is dehydrated in an ethanol series (30% 50% 70% (in PBT), 96% and 100%) and the tissue is stored at −20 °C. The following steps are as in (Almudi et al., 2019a), but noting that the proteinase K treatment is 2' long. The samples were counterstained with the nuclear stain DAPI.

Branching metrics. We computed the following metrics:

Branch density: Total accumulated pixels in a gill (RT), relative to its area (or surface, S)

$$Branch\ density = \frac{RT}{S}$$

Tip density: total number of tips (P) of a gill relative to its surface.

$$Tip\ density = \frac{P}{S}$$

Node density: total number of nodes (or branching points; NT) relative to gill's surface

$$Node\ density = \frac{NT}{S}$$

Average number of ancestors: Average of nodes between each tip and the root of the branching pattern, relative to the gill's surface square root

$$Average\ ancestors = \frac{\frac{\sum_i^n N_i}{n}}{\sqrt{S}}$$

where:

i: is the *i-th* tip,
n: is the total number of tips,
N_i: is the accumulated number of nodes up to reaching the *i-th* tip,
S: is the gill's surface.

Asymmetry in branch length: To calculate it, first we measure the length between each node and the closest tip and generate a distribution in which the number of points equals the number of tips. Once the distribution has been defined, the Fisher's asymmetry index is calculated, according to the formula:

$$As = \frac{\sum_{i=1}^{n}(x_i - \bar{x})^3}{ns^3}$$

where:

i: is the *i-th* tip,
n: is the total number of tips,
x_i: is the branch length ending at tip *i,*
s: standard deviation of the length distribution.

This is an asymmetry index of third degree which gives higher weight to extreme values and thus allows determining if the branch length is not uniform. It is non-dimensional and therefore does not need to be made relative to the gill's surface.

Correlation among ancestors and length: defined as the linear correlation coefficient between branch length (as defined above) and number of ancestors of each branch,

$$Correlation_{XN} = \frac{Cov_{XN}}{S_X S_N}$$

where:

N: is the accumulated number of nodes up to reaching a tip,
X: is the branch length ending at this tip,
S: standard deviation of the distribution of X or N,
Cov_{XN}: covariance between X and *N.*

Fractal dimension: The fractal dimension (*D*) provides a statistical index of complexity by comparing how the detail in a pattern changes with the scale at which it is measured. It is also a measure of the space-filling capacity of a pattern. To estimate *D* we have followed the Box-counting method (Napolitano et al., 2012). We consider our branching pattern as a fractal structure embedded in a 2-dimensional gill. The box-counting method basically consists in partitioning the space with a 2-dimensional fixed-grid of square boxes of equal size r. The number *N(r)* of nonempty boxes of size *r* needed to cover the fractal structure depends on *r*:

$$\mathrm{N(r)} - \mathrm{r}^{-\mathrm{D}}$$

As our images are 512 × 512 pixels, we reduce scale on the basis of $r = \frac{1}{2^n}$ from 1/2 to 1/512. The box counting algorithm hence counts the number *N(r)* for different values of *r* and plot the log of *N(r)* versus the log of the actual box size *r*. The value of the box-counting dimension *D* is estimated as the Richardson's plot best fitting curve slope:

$$-D = \lim_{r \to 0} \frac{\log N(r)}{\log r}$$

Principal component analysis (PCA). We have performed a PCA using *princomp()* function from the *stats* library in *R software*. It follows the *Spectral decomposition method* which examines the covariances/correlations between variables to estimate the linear combination of them that get to explain the maximum of variance for each consecutive component.

First, we included all our 7 previously described metrics to produce the natural morphospace PCA, but the "Correlation among ancestors and length" metric turned out to have too much relevance in the PCA. Consequently, we analyzed this variable further. We found that the intragroup (species) variance was very high, meaning that this metric is very sensitive to small changes in the branch length distribution across the gill, that could happen randomly, and could lead to a non useful rearrangement of data in the PCA, so we finally decided to remove it from the PCA.

Statistical analysis was developed in R software. Multinomial regression was implemented through *multinom* function, *nnet* library (Venables and Ripley, 2002), with all defaults settings. Pairwise comparisons were performed with *TukeyHSD* function from *agricolae* library (de Mendiburu, 2019).

dSCA pseudo-code. Description of the dSCA algorithm implemented in this work.

```
//MAX - > maximum radius of influence of M.
//KILL - > maximum reach of a branch.
//CREC - > growth in length of each segment per iteration.
//vel - > velocity of Ms in their random motion.
//coordinates of attractors (M) and of seed branch.

Program SCA {
    load starting parameters;
    initialize variables (time, M number);
    enter the coordinates of seed (initial branch);

    while(number of M > 0){
        graphic output M and branches;
        time++;

        for(all M){
            associate M to closest branch;
            if(distance(M,closest branch) < KILL{
                remove M;
                M number--;
            }
            if(distance(M,closes branch) < MAX{
                M attracts the branch
                update the growth vector of this branch;
            }
        }
        for (all branches){
            if (there are attracting M){
                branch or grow:
                extend a new branch of length CREC along direction v;
            }
        }
        while(vel) for(all M) move M randomly;
        if(number of M == 0){
            save data;
            stop and finish program;
            }
        }
    }
```

The full set of images (natural gills and SCA generated patterns) and extracted datasets are provided as Supplementary Material. Software (segmentation macros, raw metrics generating algorithm and spatial colonization algorithm) is available through GitHub (https://github.com/Carlosmarbla/Spatial-Colonization-Algorithm, and see Supplementary Materials).

Funding

Grants: 1455906 (National Science Foundation, USA) to DHF; TIN2017-89842P (MINECO/AEI, Spain, co-financed by FEDER funds (EU)) to FJ and MCL; 657732 (Marie Sklodowska-Curie Program, EU) to IA; BFU2015-66040-P and PGC2018-093704-B-I00 (MINECO/AEI, Spain co-financed by FEDER funds (EU)) to FC and institutional grant MDM-2016-0687 (MINECO/AEI, Spain co-financed by FEDER funds (EU)) in which FC is participant researcher.

Author's contributions

FC conceived the study and obtained major funding; FC and FJ supervised the study; FJ and ARS wrote software for the SCA algorithm; CMB wrote macros for ImageJ (processing and segmentation) of gill images; ARS and TN developed metrics for geometry analysis; TN carried out statistical analysis; ARS, FC, CMB, IA, DHF, J-LG generated data; FC, ARS, FJ, TN, DHF, J-LG, MCL, DBB analyzed data and results; FC wrote the manuscript with the help of DBB and inputs from all authors.

Declaration of competing interest

The authors declare no competing interests.

Appendix A. Supplementary data

Supplementary data to this article can be found online at https://doi.org/10.1016/j.ydbio.2020.02.005.

References

Almudi, I., Martin-Blanco, C.A., Garcia-Fernandez, I.M., Lopez-Catalina, A., Davie, K., Aerts, S., Casares, F., 2019a. Establishment of the mayfly Cloeon dipterum as a new model system to investigate insect evolution. EvoDevo 10, 1.

Almudi, I., Vizueta, J., de Mendoza, A., Wyatt, C., Marletaz, F., Firbas, P., Feuda, R., Masiero, G., Medina, P., Alcaina, A., et al., 2019b. Genomic adaptations to aquatic and aerial life in mayflies and the origin of wings in insects. BioRxiv.

Arganda-Carreras, I., Kaynig, V., Rueden, C., Eliceiri, K.W., Schindelin, J., Cardona, A., Sebastian Seung, H., 2017. Trainable Weka Segmentation: a machine learning tool for microscopy pixel classification. Bioinformatics 33, 2424–2426.

Craig, D.A., 1990. Behavioral hydrodynamics of Cloeon dipterum larvae (Ephemeroptera: Baetidae). J. North Am. Benthol. Soc. 9, 346–357.

Davies, J.A., 2002. Do different branching epithelia use a conserved developmental mechanism? Bioessays 24, 937–948.

de Mendiburu, F., 2019. Agricolae: Statistical Procedures for Agricultural Research. R Package Version 1.3-1.

Ghabrial, A.S., Levi, B.P., Krasnow, M.A., 2011. A systematic screen for tube morphogenesis and branching genes in the Drosophila tracheal system. PLoS Genet. 7, e1002087.

Glenny, R.W., 2011. Emergence of matched airway and vascular trees from fractal rules. J. Appl. Physiol. 110 (1985), 1119–1129.

Hannezo, E., Scheele, C., Moad, M., Drogo, N., Heer, R., Sampogna, R.V., van Rheenen, J., Simons, B.D., 2017. A unifying theory of branching morphogenesis. Cell 171, 242–255 e227.

Iber, D., Menshykau, D., 2013. The control of branching morphogenesis. Open Biol. 3, 130088.

Kim, H.Y., Varner, V.D., Nelson, C.M., 2013. Apical constriction initiates new bud formation during monopodial branching of the embryonic chicken lung. Development 140, 3146–3155.

Kitaoka, H., Suki, B., 1997. Branching design of the bronchial tree based on a diameter-flow relationship. J. Appl. Physiol. 82 (1985), 968–976.

Kondo, S., Miura, T., 2010. Reaction-diffusion model as a framework for understanding biological pattern formation. Science 329, 1616–1620.

Kukalova-Peck, J., 1985. Ephemeroid wing venation based upon new gigantic Carboniferous mayflies and basic morphology, phylogeny, and metamorphosis of pterygote insects (Insecta, Ephemerida). Can. J. Zool. 63, 933–955.

Mandelbrot, B.B., 1983. The Fractal Geometry of Nature. W.H. Freeman, New York.

Menshykau, D., Blanc, P., Unal, E., Sapin, V., Iber, D., 2014. An interplay of geometry and signaling enables robust lung branching morphogenesis. Development 141, 4526–4536.

Menshykau, D., Michos, O., Lang, C., Conrad, L., McMahon, A.P., Iber, D., 2019. Image-based modeling of kidney branching morphogenesis reveals GDNF-RET based Turing-type mechanism and pattern-modulating WNT11 feedback. Nat. Commun. 10, 239.

Metzger, R.J., Krasnow, M.A., 1999. Genetic control of branching morphogenesis. Science 284, 1635–1639.

Metzger, R.J., Klein, O.D., Martin, G.R., Krasnow, M.A., 2008. The branching programme of mouse lung development. Nature 453, 745–750.

Napolitano, A., Ungania, S., Cannata, V., 2012. Fractal dimension estimation methods for biomedical images. In: MATLAB – A Fundamental Tool for Scientifi c Computing and Engineering Applications, vol. 3, pp. 161–178.

Nelson, T.R., Manchester, D.K., 1988. Modeling of lung morphogenesis using fractal geometries. IEEE Trans. Med. Imag. 7, 321–327.

Nelson, T.R., West, B.J., Goldberger, A.L., 1990. The fractal lung: universal and species-related scaling patterns. Experientia 46, 251–254.

Nogawa, H., Ito, T., 1995. Branching morphogenesis of embryonic mouse lung epithelium in mesenchyme-free culture. Development 121, 1015–1022.

Ochoa-Espinosa, A., Affolter, M., 2012. Branching morphogenesis: from cells to organs and back. Cold Spring Harb. Perspect. Biol. 4.

Okenve-Ramos, P., Llimargas, M., 2014. Fascin links Btl/FGFR signalling to the actin cytoskeleton during Drosophila tracheal morphogenesis. Development 141, 929–939.

Ribeiro, C., Ebner, A., Affolter, M., 2002. In vivo imaging reveals different cellular functions for FGF and Dpp signaling in tracheal branching morphogenesis. Dev. Cell 2, 677–683.

Riek, E.F., 1973. The classification of the Ephemeroptera. In: First International Conference on Ephemeroptera, pp. 160–178. Leiden, The Netherlands.

Rueden, C.T., Schindelin, J., Hiner, M.C., DeZonia, B.E., Walter, A.E., Arena, E.T., Eliceiri, K.W., 2017. ImageJ2: ImageJ for the next generation of scientific image data. BMC Bioinf. 18, 529.

Runions, A., Fuhrer, M., Lane, B., Federl, P., Rolland-Lagan, A.G., Prusinkiewicz, P., 2005. Modeling and visualization of leaf venation patterns. ACM Trans. Graph. 24, 702–711.

Runions, A., Brendan, L., Prusinkiewicz, P., 2007. Modeling trees with a space colonization algorithm. In: Ebert, D., Mérillou, S. (Eds.), Eurographics Workshop on Natural Phenomena. The Eurographics Association.

Sato, M., Kornberg, T.B., 2002. FGF is an essential mitogen and chemoattractant for the air sacs of the drosophila tracheal system. Dev. Cell 3, 195–207.

Spurlin 3rd, J.W., Nelson, C.M., 2017. Building branched tissue structures: from single cell guidance to coordinated construction. Philos. Trans. R. Soc. Lond. B Biol. Sci. 372.

Sweeney, B.W., Funk, D.H., Camp, A.A., Buchwalter, D.B., Jackson, J.K., 2018. Why adult mayflies of Cloeon dipterum (Ephemeroptera : Baetidae) become smaller as temperature warms. Freshw. Sci. 37, 64–81.

Varner, V.D., Nelson, C.M., 2017. Computational models of airway branching morphogenesis. Semin. Cell Dev. Biol. 67, 170–176.

Venables, W.N., Ripley, B.D., 2002. Modern Applied Statistics with S, fourth ed. Springer, New York.

Volckaert, T., Campbell, A., Dill, E., Li, C., Minoo, P., De Langhe, S., 2013. Localized Fgf10 expression is not required for lung branching morphogenesis but prevents differentiation of epithelial progenitors. Development 140, 3731–3742.